Histamine interferes with the early visual processing in mice

Authors: Matteo Tripodi[1], Hiroki Asari*[1]

Affiliations:

1. Epigenetics and Neurobiology Unit, EMBL Rome, European Molecular Biology Laboratory, Monterotondo, 00015, Italy

***Corresponding author:** Hiroki Asari, E-mail: asari@embl.it

Author contributions: M.T. and H.A. designed the study; M.T. performed experiments; M.T. and H.A. analyzed the results; and M.T. and H.A. wrote the manuscript.

Competing interests: The authors declare no competing financial interests.

Key words: retinal ganglion cells; lateral geniculate nucleus; histaminergic modulation; tuberomammillary nucleus.

Acronyms: AAV, adeno-associated virus; ANOVA, analysis of variance; DLP, digital light processing; DRN, dorsal raphe nucleus; HDC, histidine decarboxylase; GABA, γ-aminobutyric acid; IQR, interquartile range; IR, infrared; LED, light emitting diode; LGN, lateral geniculate nucleus; OT, optic tract; PFA, paraformaldehyde; PSAM/PSEM, pharmacologically selective actuator/effector module; RF, receptive field; RGC, retinal ganglion cell; STA, spike-triggered average; tSNE, t-distributed Stochastic Neighbor Embedding; UV, ultraviolet.

Abstract

Sensory processing is dynamically modulated by an animal's behavior and internal states. Growing evidence suggests that such modulation starts from early stages, even at the retina, but the underlying mechanisms remain elusive. Combining pharmacological and chemogenetic tools with single-unit extracellular recordings in awake head-fixed mice, here we identified that the visual responses of retinal ganglion cells and the lateral geniculate nucleus were both made weaker and slower by histaminergic projections from the tuberomammillary nucleus of the posterior hypothalamus. The observed changes in the visual responses were, however, not directly linked with histaminergic modulation of pupil dynamics or locomotion behavior. Our computational modelling analysis instead suggests neuronal circuit effects, such as gain modulation via the histamine H1 receptors in the retina. As nocturnal animals, facilitation of visual processing at low histamine level is ethologically beneficial for mice to respond faster to visual threats when animals are less active during daytime.

Introduction

In the mammalian brain, histaminergic neurons are exclusively located in the tuberomammillary nucleus (TMN) and surrounding areas of the posterior hypothalamus (Haas and Panula, 2003). They express histidine decarboxylase (HDC) and innervate widely across the brain (Lin et al., 2023), including the retina (Gastinger et al., 1999; Repérant et al., 2007; Warwick et al., 2024). These neurons remain silent during sleep, but increase their firing during wakefulness and reach their maximal activity at the state of high vigilance, much as other monoaminergic systems do, such as the serotonergic neurons in the dorsal raphe nucleus (DRN) of the brain stem (Lin et al., 2023; Takahashi et al., 2006; Thakker, 2011). Brain histamine exerts its effects via three types of receptors: the H1 and H2 receptors mediate excitation of postsynaptic cells, while the H3 receptors serve as an auto-receptor to presynaptically inhibit histamine release (Haas and Panula, 2003). The central histaminergic

system has been implicated in regulating an animal's state and a broad range of behavior, including the sleep-wake cycle (John et al., 2004; Mochizuki et al., 1992), arousal (Parmentier et al., 2002; Scammell et al., 2018), suppression of food intake (Khouma et al., 2023; Valdés et al., 2010; Wang et al., 2015) and learning (Kamei et al., 1993; Klapdor et al., 1994; Orsetti et al., 2001; Rubio et al., 2002). Histaminergic neurons, however, corelease γ-aminobutyric acid (GABA) and interact with other neuromodulatory systems, such as the cholinergic and serotonergic systems (Brown et al., 2002; Khateb et al., 1995; Lin et al., 2023). This makes it difficult to dissect the effects of histamine by itself on neural circuit functions. In particular, histaminergic modulation of sensory processing remains largely elusive (Lee and Dan, 2012; McCormick et al., 2020).

The retina performs the first stage of visual processing, and conveys visual information to the brain via spike trains of retinal ganglion cells (RGCs). Growing evidence supports that the activity of RGCs is correlated with various behavioral measures, such as locomotion and pupil size (Schröder et al., 2020; Liang et al., 2020; Reggiani et al., 2023; Boissonnet et al., 2023), pointing to a more dynamic role of the retina than is assumed for a deterministic processor. The vertebrate retina is part of the central nervous system equipped with both intrinsic and extrinsic neuromodulation mechanisms, much as other brain regions are (Lee and Dan, 2012; McCormick et al., 2020). For instance, dopamine is synthesized and released by a group of retinal amacrine cells under the control of circadian rhythm, and contributes to adjusting the retinal circuitry for rod or cone vision by modulating gap-junction couplings (Bloomfield and Völgyi, 2009). Such retinal intrinsic mechanisms of neuromodulation are, however, much slower than needed to modulate retinal function to follow rapid behavioral changes. To this end, the retina seems to exploit the centrifugal system to receive inputs from a variety of brain regions in a species-specific manner (Repérant et al., 2007). For example, histaminergic and serotonergic projections from TMN and DRN, respectively, have been anatomically described in the mammalian retina (Gastinger et al., 1999; Greferath et al., 2009; Labandeira-Garcia et al., 1990; Warwick et al., 2024). However, compared to the isthmo-optic

pathway in birds (Wilson and Lindstrom, 2011) or the olfacto-retinal circuit in fish (Esposti, et al., 2013), little is known about the function of the mammalian centrifugal system.

Combining in vivo single-unit extracellular recordings from either the lateral geniculate nucleus (LGN) or the optic tract (OT) with pharmacological and chemogenetic tools, here we explored how histamine affects the early visual processing in awake head-fixed mice. During the recording sessions, we simultaneously monitored the subject animal's behavior, such as pupil dynamics and locomotion, to better correlate the effects of histamine on the visual response properties with those on the behavioral measures. We also took a computational approach to clarify the net effect of histamine on the visual responses from functional viewpoints. Because visual processing in the brain fully relies on the signals from the retina, characterization of the retinal operation in vivo is indispensable to better understand how the visual system works.

Results

Histamine leads to weaker and slower visual responses in the mouse lateral geniculate nucleus

To investigate how histamine influences the mouse visual system, we first performed in vivo single-unit extracellular recordings from the lateral geniculate nucleus (LGN) in awake head-fixed mice, and compared the visual response properties of the recorded cells before and after perturbing the central histaminergic system (Figure 1A; see Methods for details). Stimulus ensemble statistical techniques ("reverse correlation"; Chichilnisky, 2001) were employed to systematically characterize the visual response properties of the recorded cells in the framework of a linear-nonlinear cascade model (Boissonnet et al., 2023). In particular, using full-field white-noise stimuli, we analyzed histaminergic effects on 1) the linear temporal filter, estimated by the spike-triggered average (STA) stimulus, i.e., the mean stimulus that triggered spiking responses; and 2) the static nonlinear gain function, i.e., an instantaneous mapping of

79 the STA output to the neural responses (Figure 1B). We also functionally mapped the cells'
80 receptive field (RF) by calculating the linear spatial filter from the responses to random binary
81 "checkerboard" stimuli, where the contrast of each spatial location was randomly and
82 independently inverted over time. To manipulate the histaminergic system, we used two
83 different approaches (Supplementary Figure 1). The first was the chemogenetic activation of
84 the central histaminergic system (Magnus et al., 2011). We injected cre-dependent adeno-
85 associated viruses (AAVs) carrying pharmacologically selective actuator module (PSAM)-
86 5HT3HC channels into the tuberomammillary nucleus (TMN) of the posterior hypothalamus in
87 histidine decarboxylase (HDC)-cre transgenic mice, and then achieved selective activation of
88 the target neurons by systemic administration of the pharmacologically selective effector
89 molecule (PSEM). The second approach was the use of pharmacological tools in wild-type
90 mice (Thakkar, 2011). Specifically, we used chlorphenamine (5 mg/kg), an antagonist of a
91 postsynaptic histamine receptor H1; and ciproxifan (12 mg/kg), an antagonist of the H3 auto-
92 receptor that presynaptically inhibits histamine release. These drugs effectively down- and up-
93 regulate the action of histamine in the nervous system, respectively. Thus, resulting changes
94 in visual processing, if any, were expected to be in opposite directions.

95 Upon chemogenetically activating HDC+ neurons in TMN, we found that LGN neurons
96 generally showed weaker and slower visual responses (Figure 1C,F; N=58 from 3 animals).
97 The mean firing rate during the visual stimulation significantly reduced (median, -5.0 Hz;
98 interquartile range (IQR), 9.9 Hz; p(U-test)<0.001); and the response gain also significantly
99 decreased (median, -41%; IQR, 54%; p(U-test)<0.001) that we computed as the ratio of the
100 estimated static nonlinearity functions before and after PSEM injection. The temporal filter
101 became elongated regardless of their functional cell types (Supplementary Figure 2), leading
102 to significantly longer peak latencies (median, +32 ms; IQR, 27 ms; p(U-test)<0.001) and lower
103 peak frequencies (median, -16%; IQR, 5 %; p(U-test)=0.01).

104 Consistent results were obtained when histamine release was pharmacologically up-
105 regulated. Specifically, after the application of ciproxifan (H3 antagonist; Figure 1D,G; N=48

106 from 2 animals), we found significantly reduced mean firing rates (median, -3.7 Hz; IQR, 5.0
107 Hz; p(U-test)<0.001) and response gain (median, -30%; IQR, 52%; p(U-test)=0.003), and
108 significantly longer peak latency (median, +17 ms; IQR, 13 ms; p(U-test)<0.001) and lower
109 peak frequency (median, -9%; IQR, 14%; p(U-test)<0.001) of the linear temporal filters. These
110 effects of the pharmacological treatment were less prominent than those of the chemogenetic
111 manipulation (Figure 1I-L), except for the changes in the receptive field size where the
112 reduction reached the statistically significant level with ciproxifan (median, -26%; IQR, 38 %;
113 p(U-test)=0.004, N=28 from 2 animals) but not with the chemogenetic manipulation (median,
114 -11%; IQR, 32 %; p(U-test)=0.11, N=19 from 2 animals; Supplementary Figure 3A-F).

115 In contrast, chlorphenamine (H1 antagonist) led to marginal changes in the visual
116 response properties of LGN neurons in the opposite direction (Figure 1E,H; N=116 from 3
117 animals). We observed a tendency towards an increased mean evoked firing rate (median,
118 +1.0 Hz; IQR, 7.2 Hz; p(U-test)=0.09) and response gain (median, +13%; IQR, 87%; p(U-
119 test)=0.3), and facilitated response kinetics with significantly higher peak frequency of the
120 linear temporal filter (median, +4%; IQR, 15%; p(U-test)=0.03) but no significant changes in
121 its peak latency (median, 0 ms; IQR, 5 ms; p(U-test)=0.7) or the receptive field size (median,
122 +5%; IQR, 34 %; p(U-test)=0.08, N=38 from 3 animals; Figure 1I-L and Supplementary Figure
123 3A-F). Taken together, these results indicate that histamine reduces the response gain and
124 slows down the response kinetics in the mouse LGN.

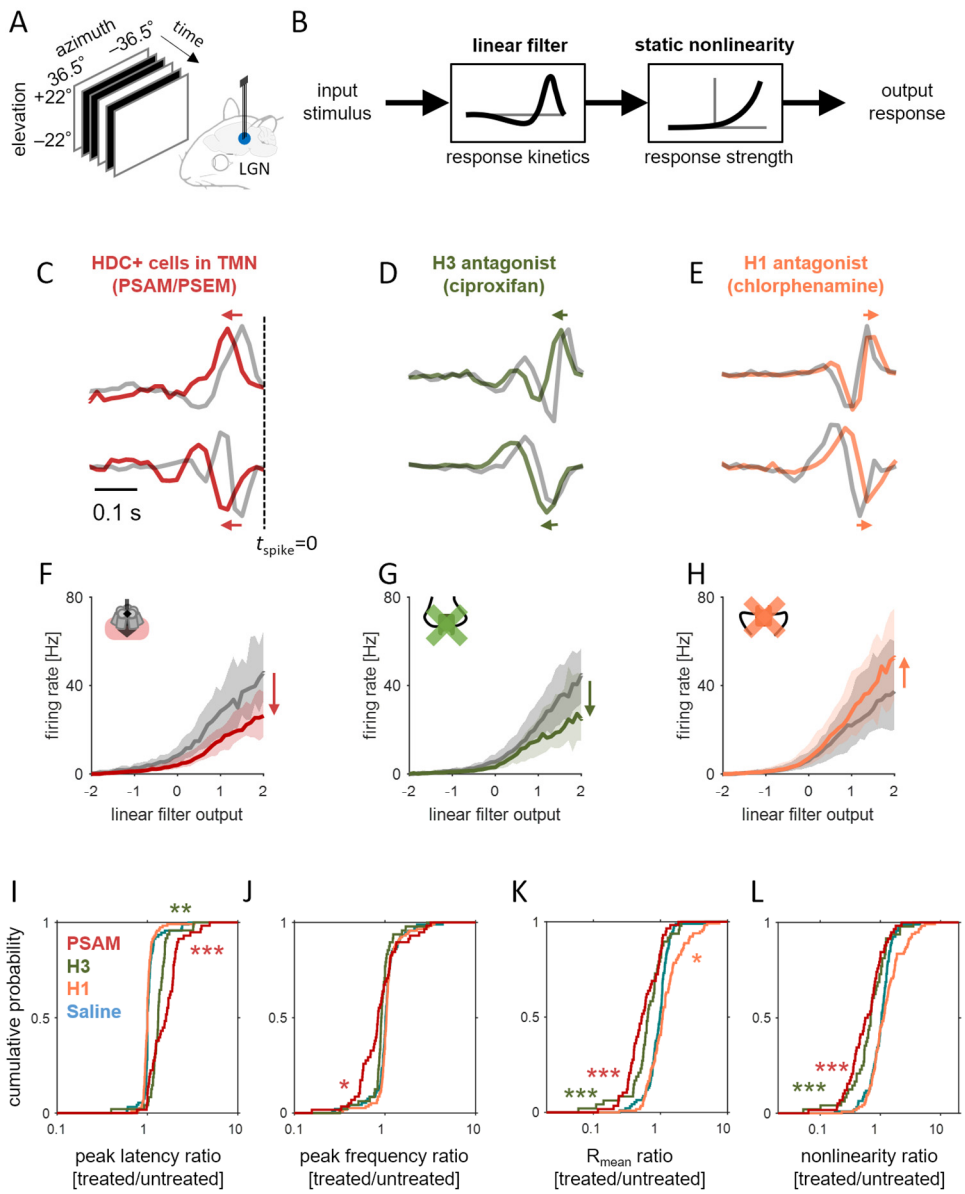

Figure 1: Histamine made the visual responses of LGN weaker and slower in awake head-fixed mice. *A,B*: Schematic diagram of LGN recordings (A) and linear-nonlinear cascade model (B). Reverse-correlation was used to estimate the linear filter and static nonlinearity that represent response kinetics and strength, respectively. *C*: Linear filters of two representative LGN cells before (gray) and after chemogenetic activation of HDC+ cells in TMN (red). *D,E*: Representative LGN linear filters before (gray) and after pharmacological treatment (D, 12 mg/kg ciproxifan, green; E, 5 mg/kg chlorphenamine, orange). *F-H*: Static nonlinearities averaged across LGN population before and after treatment in corresponding colors (F, chemogenetics, N=58 from 3 animals; G, ciproxifan, N=48 from 2 animals; H, chlorphenamine, N=116 from 3 animals): line, median; gray shade, 25 and 75 percentiles. *I-L*: Cumulative distributions of response feature ratio before and after each treatment (in corresponding color): peak latency (I) and frequency (J) of the linear temporal filters, mean evoked firing rate during stimulation (K), and static nonlinearity (i.e., response gain; L). One-way analysis of variance (ANOVA) with Tukey-Kramer correction was used to compute the p-value against saline control (blue, N=93 from 3 animals): *, p<0.05; **, p<0.01; ***, p<0.001.

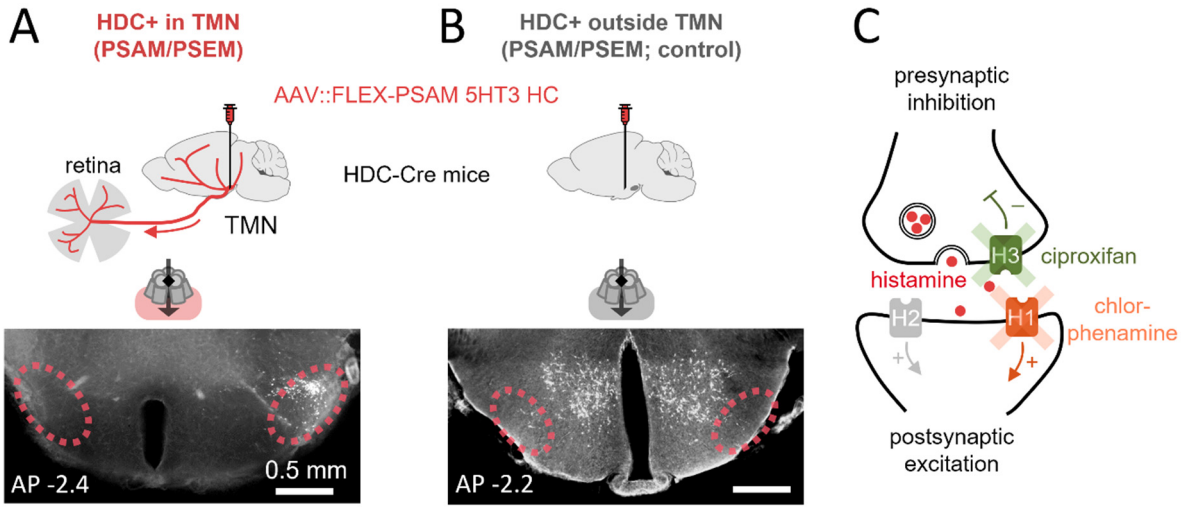

Supplementary Figure 1: Pharmacological and chemogenetic approaches to manipulate the central histaminergic system in the mouse brain. *A,B*: Viral delivery of PSAM 5HT3HC channel to HDC+ cells in the TMN (marked with dotted lines) of the posterior hypothalamus (A) or those in the anterior hypothalamus (B; control). *C*: Schematic diagram of histamine receptor localizations and their cellular function. Chlorphenamine blocks the postsynaptic receptor H1 (orange) that mediates the action of histamine postsynaptically, while ciproxifan blocks the auto-receptor H3 (green) that inhibits presynaptic histamine release.

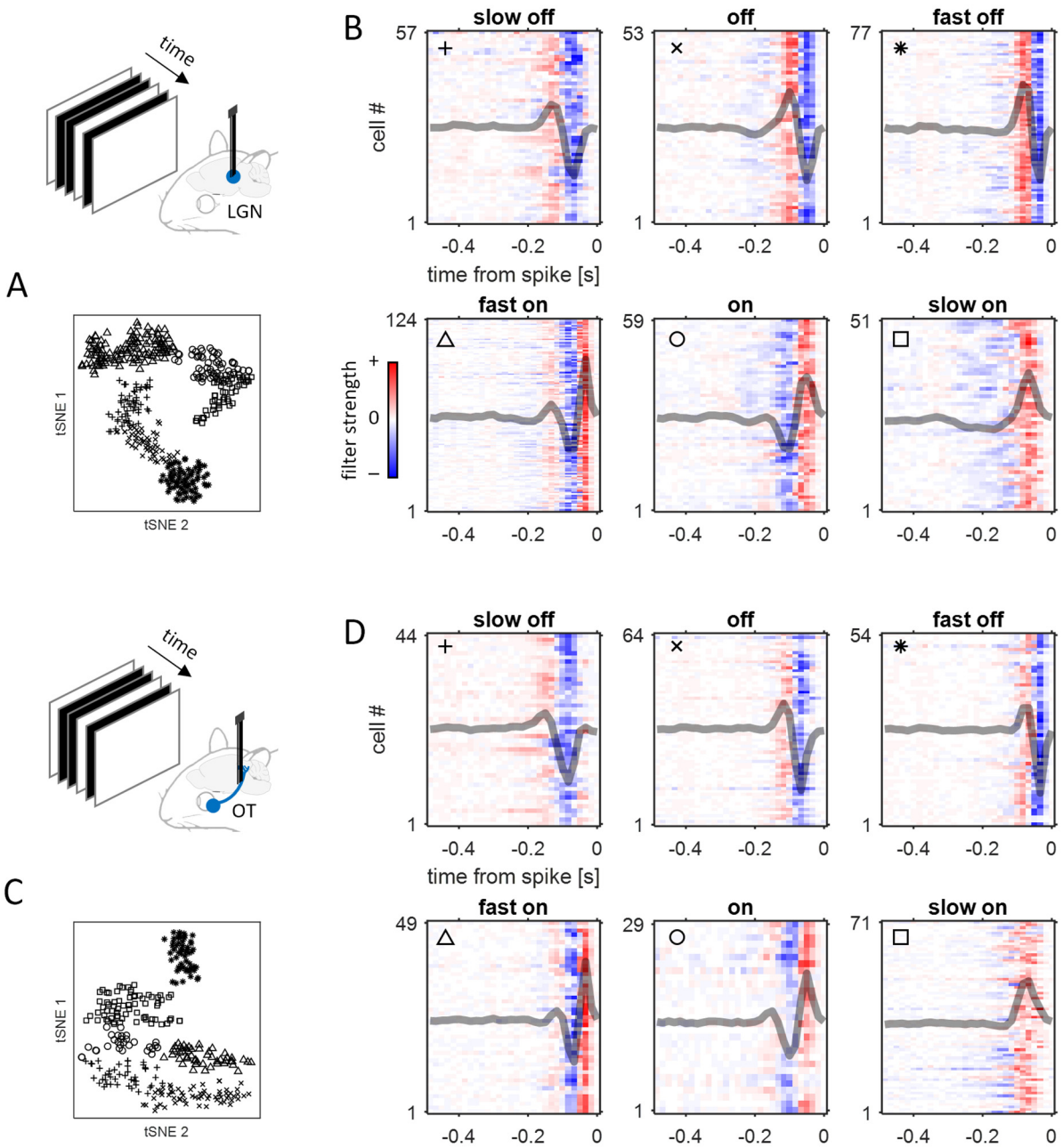

Supplementary Figure 2: Functional classification of LGN/RGC visual response types. *A*: t-SNE embedding of the STAs of LGN cells. Different markers are used for distinct response categories (shown in B). *B*: Each panel represents one of the six response categories: slow off, off, fast off, fast on, on, and slow on. In each panel, each row represents a cell's STA (color-coded with red and blue indicating positive and negative filter values, respectively); and the overlaid gray line shows the average STAs in each response type. *C,D*: Corresponding data for RGCs obtained by in vivo optic tract (OT) recordings methods.

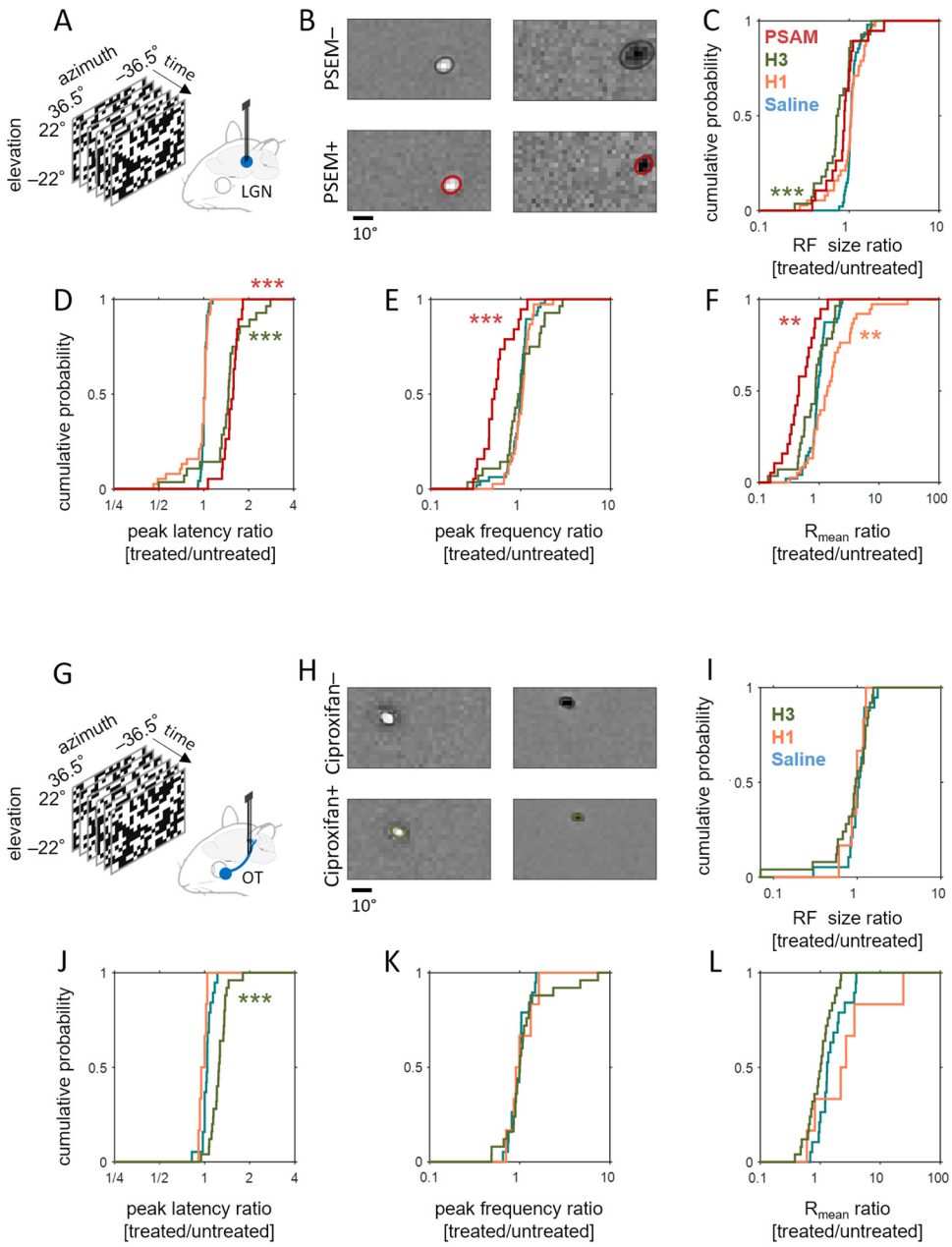

Supplementary Figure 3: Histamine reduced the LGN but not RGC RF size. *A*: Schematic diagram of LGN recordings with white-noise "checkerboard" stimuli. *B*: Estimated spatial filter (receptive field) of two example LGN cells before (top) and after (bottom) chemogenetic activation of HDC+ cells in TMN. Note a decrease of the RF size of this OFF LGN cell (right), while no change was observed for this ON cell (left). *C-F*: Cumulative distribution of the RF size ratio of LGN cells before and after treatment (C; orange, chlorphenamine, N=38 from 3 animals; green, ciproxifan, N=28 from 2 animals; red, PSAM/PSEM for HDC+ cells in TMN, N=19 cells from 2 animals) and corresponding figure panels for the peak latency (D) and frequency (E) of the RF center dynamics as well as for the mean firing rate (F). One-way ANOVA with Tukey-Kramer correction against saline control (N=48 from 3 animals): *, $p<0.05$; **, $p<0.01$; ***, $p<0.001$. *G-L*: Corresponding figure panels for RGCs: chlorphenamine (H1 antagonist), N=6 from 3 animals; ciproxifan (H3 antagonist), N=25 from 4 animals; saline, N=18 from 3 animals.

Histaminergic modulation starts from the mouse retina

Histaminergic neurons are localized solely in the hypothalamus, most densely in TMN, and project their axons widely across the brain (Lin et al., 2023), including the mouse retina (Gastinger et al., 1999; Repérant et al., 2007; Warwick et al., 2024). To test if the observed histaminergic modulation of the visual processing in LGN originates in the retina, we next performed in vivo optic tract (OT) recordings to monitor the retinal output responses in awake head-fixed mice (Boissonnet et al., 2023) before and after manipulating the central histaminergic system (Figure 2).

Consistent with the results in LGN, chemogenetic activation of HDC+ neurons in TMN led to reduced firing (median, -13.0 Hz; IQR, 25.5 Hz; p(U-test)=0.11) with lower response gain (median, -51%; IQR, 50 %; p(U-test)=0.04); and slower response kinetics with elongated linear temporal filters in retinal ganglion cells (RGCs; peak latency change, median, 46 ms; IQR, 22 ms; p(U-test)=0.008; peak frequency change, median, -36%; IQR, 22%, p(U-test)=0.04; N=10 from 2 animals; Figure 2A,D). In contrast, no change in these response parameters was observed when targeting HDC+ populations in the anterior hypothalamus outside TMN for the PSAM/PSEM activation (firing rate change, median, -0.7 Hz, IQR, 16 Hz, p(U-test)=1; gain change, median, 0.5%, IQR, 79%, p(U-test)=1; latency change, median +2 Hz, IQR, 11 Hz, p(U-test)=0.8; frequency change, median -2.9%, IQR, 11%, p(U-test)=0.12; N=23 from 3 animals). This supports that the histaminergic modulation of the early visual system is mediated by the centrifugal projections specifically from TMN (Figure 2G-J and Supplementary Figure 1).

The effects of the pharmacological treatments were overall similar between LGN and RGCs, though certain differences existed. First, pharmacologically blocking the H3 receptors with ciproxifan led to slower response kinetics in both LGN and RGCs (latency change, median, 8 ms; IQR, 14 ms; p(Utest)<0.001; frequency change, median, -7%; IQR, 19%; p(U-test)=0.04; N=40 from 4 animals), but the firing rates and the response gain remained largely unaffected in RGCs (Figure 2B,E; firing rate change, median -0.3 Hz; IQR, 14.2 Hz; p(U-text)=0.8; gain

198 change, median, -1.3%; IQR, 68%, p(Utest)=0.8). Second, while chlorphenamine (H1
199 antagonist) drove faster kinetics with marginally higher firing in both LGN and RGCs, the
200 effects on the temporal filters were primarily on the peak frequencies in LGN (Figure 1E,H)
201 but on the peak latencies in RGCs (Figure 2C,F; latency change, median, -5 ms; IQR, 10 ms;
202 p(U-test)=0.004; frequency change, median, +4 Hz; IQR, 19 Hz; p(U-test)=0.7; firing rate
203 change, median, +2.1 Hz, IQR, 10.4 Hz; p(U-test)=0.14; gain change, median, 5%, IQR, 88%,
204 p(U-test)=0.2; N=34 RGCs from 3 animals). Finally, RGC receptive fields did not show
205 significant changes in size (Supplementary Figure 3G-L; ciproxifan, median, -4%, IQR, 54%,
206 p(U-test)=1, N=25 from 4 animals; chlorphenamine, median, ±0%, IQR, 36%, p(U-test)=1,
207 N=6 from 3 animals; saline, median, 5%, IQR, 30%, p(U-test)=0.36, N=18 from 3 animals).
208 Taken together, our electrophysiology data indicate that 1) the mouse early visual processing
209 is subject to histaminergic modulation controlled by TMN, starting from the retina; 2) histamine
210 generally suppresses the firing and slows the response kinetics; and 3) response latency and
211 frequency tuning are likely modulated by different mechanisms.

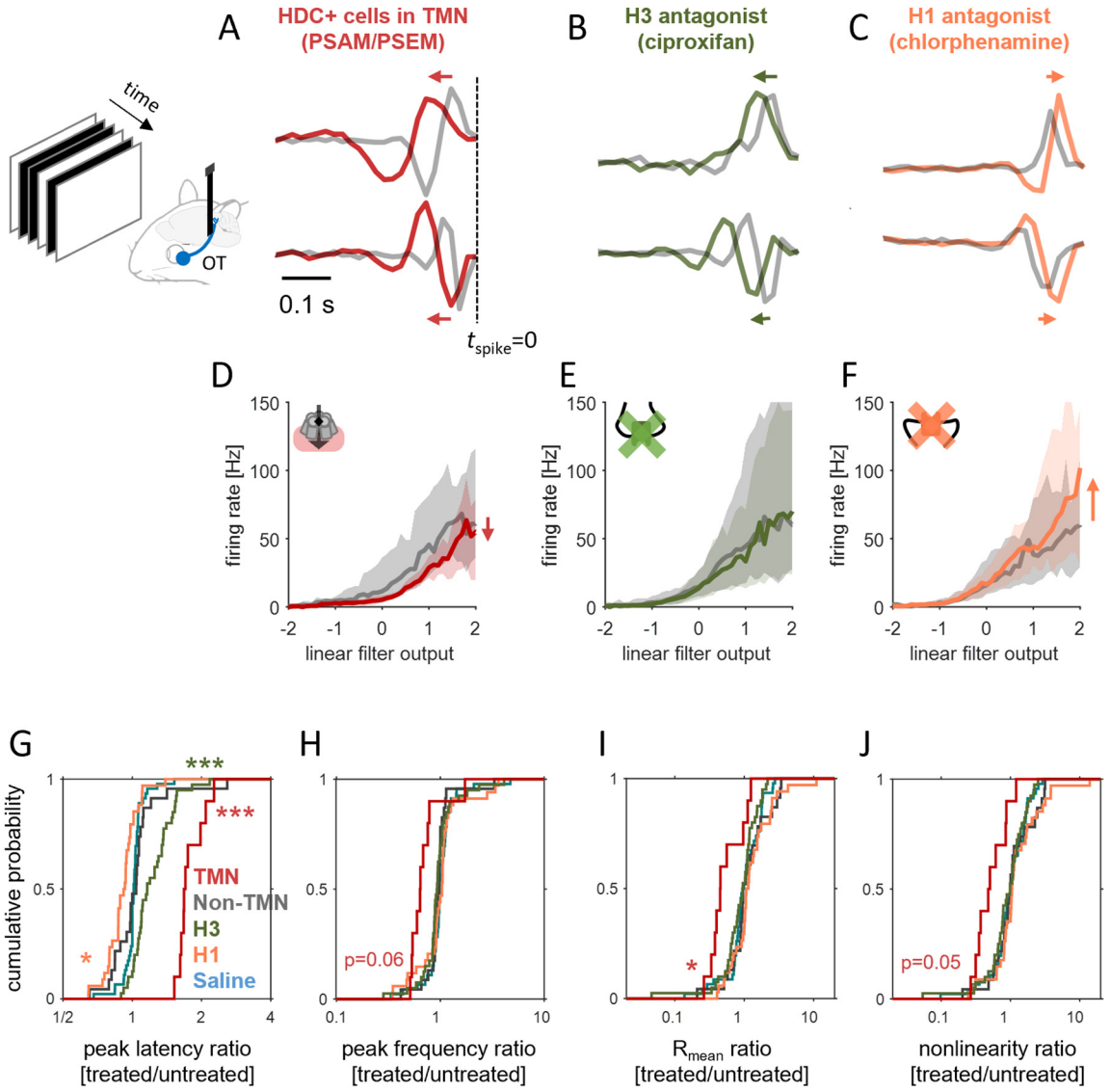

Figure 2: histamine primarily affected the visual response kinetics of RGCs. *A-C*: Linear filters of two representative RGCs before (gray) and after chemogenetic (A) or pharmacological treatment (B, ciproxifan, green; C, chlorphenamine, orange). Schematic diagram of in vivo optic tract (OT) recordings is displayed on the left. *D-F*: Static nonlinearities averaged across RGC population before and after treatment in corresponding colors (D, chemogenetics, N=10 from 2 animals; E, ciproxifan, N=40 from 4 animals; F, chlorphenamine, N=34 from 3 animals): line, median; gray shade, 25 and 75 percentiles. *G-J*: cumulative distributions of the response feature ratio before and after each treatment (in corresponding colors): peak latency (G) and frequency (H) of the linear temporal filters, mean evoked firing rate during stimulation (I), and static nonlinearity gain function (J). One-way ANOVA with Tukey-Kramer correction (chemogenetics against non-TMN targets, N=23 from 3 animals, dark gray; pharmacology against saline control, N=46 from 4 animals, blue): *, $p<0.05$; **, $p<0.01$; ***, $p<0.001$.

Pupil dynamics and locomotion are irrelevant to histaminergic modulation of early visual processing

Histamine is a potent neuromodulator implicated in various brain functions and behaviors, such as sleep-wake cycles and arousal (Haas and Panula, 2003; Thakkar, 2011). We then cannot deny the possibility that the observed histaminergic effects on the visual response properties in the mouse early visual system are by-products of behavioral modulation. For example, a larger pupil size leads to stronger responses because more photons reach the retina (Boissonnet et al., 2023). To address this issue, we examined the relationship between the histaminergic effects on the RGC/LGN visual responses and simultaneously monitored behavioral measures (Figure 3).

We first analyzed the histaminergic modulation of pupil dynamics (Figure 3A). We found pupil dilation in all 6 mice after chlorphenamine (H1 antagonist) application, but pupil constriction in 7 out of 8 animals when histamine release was enhanced by systemic injection of ciproxifan (H3 antagonist). Chemogenetic activation of the central histaminergic system, however, led to pupil dilation in most animals (4 out of 5 mice). Thus, the polarity of the changes in pupil size was not consistent with that of RGC/LGN visual responses. This suggests that the histamine-driven changes of pupil size cannot explain the modulation of the early visual responses.

We next examined how histamine affects locomotion of the head-fixed animals on the treadmill during recordings (Figure 3B,C). These mice often stayed still and moved fast ("running" at >2 cm/s) only about 20% of the time on average. In general, none of the perturbations of the histaminergic system strongly affected the time spent running in most mice (Figure 3B). When they did, however, we found that the chemogenetic activation of HDC+ neurons in TMN resulted in a substantial increase of no-running periods (2 out of 6 mice), whereas both chlorphenamine and ciproxifan led to a substantial decrease of no-running periods (2 out of 6 and 1 out of 7 mice, respectively). Furthermore, the mean running

speed during the recordings decreased upon the chemogenetic activation, whereas it varied in both directions after the pharmacological treatments (Figure 3C). Thus, changes in locomotion driven by histamine were not in agreement with the histaminergic effects on the RGC/LGN visual responses (Figures 1 and 2).

Taken together, neither pupil dynamics nor locomotion behavior was causally linked with the histaminergic modulation of the mouse early visual system. We conclude that the central histaminergic system modulates the mouse vision, effectively leading to slower and weaker responses.

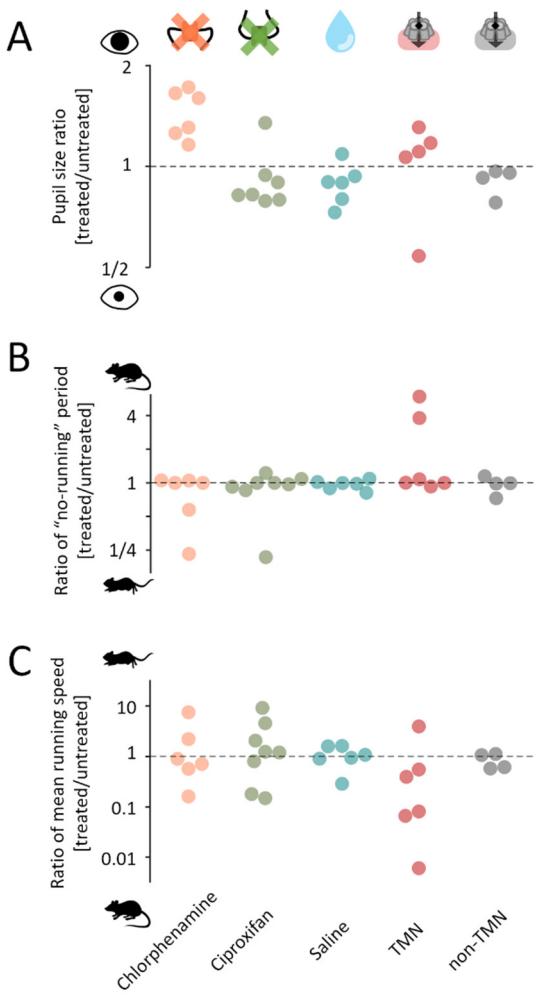

Figure 3: histaminergic modulation of pupil dynamics and locomotion behavior was not causally linked with that of RGC/LGN visual responses. *A*: the ratio of the average pupil size before and after treatment (in corresponding colors). *B*: the ratio of the "no-running" periods (threshold, 2 cm/s) before and after treatment. *C*: the ratio of the average locomotion speed during recording sessions before and after treatment.

Response gain modulation is more strongly correlated with peak latency modulation than with peak frequency modulation

What are the mechanisms underlying the histaminergic modulation of early visual processing? To address this question, we next took a computational approach to examine the relationship between different aspects of the visual response properties that we identified to be affected by histamine (Figure 4). In particular, we simulated the activity of an integrate-and-fire neuron with Poisson spiking and refractoriness in response to white-noise input stimuli (Figure 4A), and processed the output spike trains in the framework of the linear-nonlinear cascade model to characterize the simulated response properties in the same way as the experimental data (Figure 1A). Here we varied two model parameters, gain and resting baseline, to examine the effects of their changes on the following four aspects of the simulated responses: spike counts, the peak latency and frequency of the estimated linear temporal filter, and the slope of the estimated static nonlinearity expressed as half-wave rectification. The rest model parameters were fixed in all simulations, including the underlying linear filter given by a trigonometric function with logarithmic scale in time, and the refractory period filter given by an exponential function. The spike threshold was drawn from a random uniform distribution ranging from 0 to 1 for each time point to approximate the Poisson spiking properties.

When the model neuron had a higher gain or higher resting baseline, subthreshold signal reached the spike threshold faster and more frequently; hence, total spike counts became higher (Figure 4B) and the peak latency of the estimated linear temporal filter appeared shorter (Figure 4C). In contrast, the apparent peak frequency of the simulated responses was dependent more strongly on the resting baseline than on the gain (Figure 4D). These changes in the estimated linear temporal filter properties were consistent with the experimental observation, where the magnitude of the response gain modulation by histaminergic perturbation was significantly correlated with that of the peak latency modulation

292 (Figure 4F,H), but much less with that of the peak frequency modulation (Figure 4G,I). This
293 agreement between the observed and simulated data indicates that, despite the simplicity, our
294 model captures aspects of neuronal response modulation to a first approximation.

295 The model analysis supports that the histaminergic effects on RGCs should involve at
296 least gain and baseline modulations. First, the H1 receptors likely mediate the gain modulation
297 in RGCs, given that chlorphenamine (H1 antagonist) led to changes in the peak latency but
298 not the peak frequency, along with changes in the estimated static nonlinearity largely by
299 scaling (Figure 2). Second, the peak frequency was modulated as well as the peak latency of
300 RGCs upon chemogenetic activation of HDC+ neurons in TMN, accompanied by a shift of the
301 estimated static nonlinearity. This implies changes in the baseline resting potential of the cells.
302 Blocking the H3 receptors, however, led to changes in the RGC response kinetics without
303 much affecting the mean firing rates. Furthermore, the net effects of histamine perturbations
304 on LGN responses were more diverse (Figure 1) and not fully explainable by the simple model
305 (Figure 4). Thus, we expect that mechanisms besides gain and baseline modulations are also
306 involved, such as neural circuit effects through retinal amacrine cells for example (Horio et al.,
307 2018).

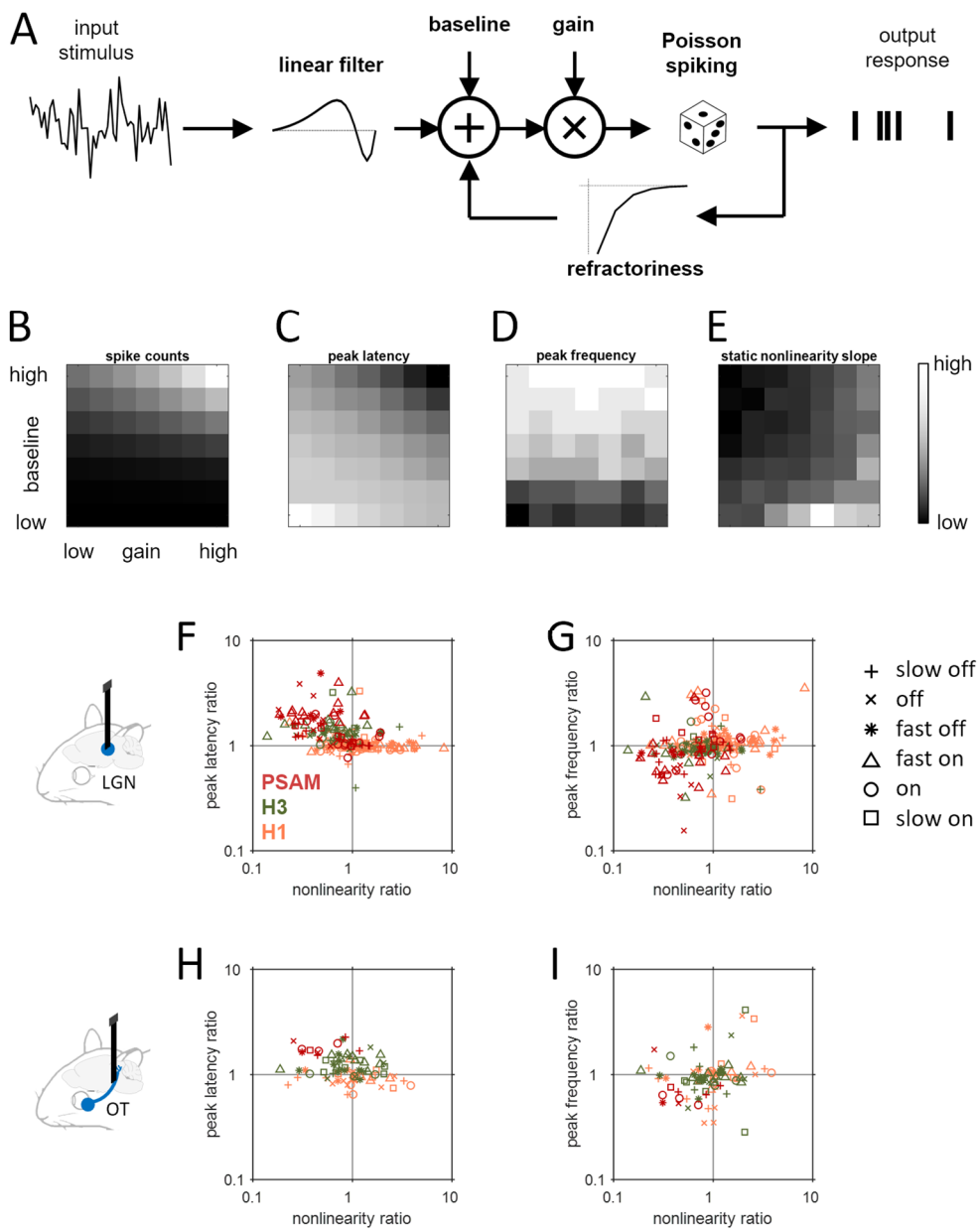

Figure 4: Gain modulation accompanies the peak latency modulation but not the peak frequency modulation via histaminergic effects. *A-E*: Using a computational model outlined in A, here we examined the consequences of varying the baseline and gain levels on the response features, such as spike counts (B), peak latency (C) and frequency (D) of the estimated linear filter from the simulated responses, and slope of static nonlinear gain function of the model neuron (E). See Methods for details. *F,G*: Relationship between the magnitudes of the gain modulation and response kinetics modulation by perturbing the histaminergic system for LGN neurons (chemogenetics, red; ciproxifan, green; chlorphenamine, orange; N=222 from 8 animals). Cell types are indicated by different markers (Supplementary Figure 2). A stronger correlation was found for the peak latencies (F, R = –0.42, p<0.001) than for the peak frequencies (G, R = 0.17, p=0.01). *H,I*: corresponding figure panels for RGC responses (N=84 from 9 animals). Significant correlation to the gain modulation was found for the peak latency modulation (R = –0.25, p = 0.02), but not for the peak frequency modulation (R= 0.20, p = 0.07).

Discussion

Here we provide in vivo electrophysiological evidence for histaminergic modulation of the mouse early visual system: the more the histamine released, the slower and weaker the LGN and RGC visual responses in awake head-fixed mice (Figures 1 and 2). This is opposite from what one would expect for the effect of histamine, given that the level of brain histamine typically increases as animals become more aroused (Thakker, 2011). At the behavioral level, antihistamine drugs lead to drowsiness in humans, impairing sensory processing (van Ruitenbeek et al., 2009). At the neurophysiological level, it has been shown that histamine leads to slow depolarization of LGN relay cells in cats and guinea pigs (McCormick and Williamson, 1991; Uhlrich et al., 2002). Histamine was thus expected to facilitate visual processing, unlike what our observations indicated. These discrepancies may arise from two reasons. First, the effects of histamine can be species-specific. In particular, many prey species often sleep with their eyes open, including mice. Furthermore, as nocturnal animals, mice are less active during daytime. Thus, facilitating visual responses at low histamine level may be ethologically beneficial for mice to respond faster to visual threats during daytime, especially when mice are dormant. Future studies in the context of sleep-wake cycles as well as in diurnal animals will give further insights into this question.

Second, our unexpected results may be due to differences in experimental conditions. Electrophysiological studies on neuromodulation were conventionally conducted in vitro or in anesthetized animals (McCormick and Williamson, 1991; Uhlrich et al., 2002; Warwick et al., 2024). It has been shown, though, that substantial differences exist in the early visual processing between awake and anesthetized conditions (Durand et al., 2016), including the retinal output (Boissonnet et al., 2023). Here we took a computational modelling approach to better understand the net effect of histamine from functional viewpoints, rather than pursuing the underlying biophysical mechanisms. We suggest that the H1 receptors mediate gain modulation in RGCs: chlorphenamine (H1 antagonist) affected the response latency but not the frequency tuning (Figure 2), a distinctive feature of gain modulation identified by our

350 computational modelling analysis (Figure 4). This action of histamine does not have to be
351 directly on RGCs expressing the H1 receptors, but can be mediated indirectly by circuit
352 mechanisms. Indeed, histamine affects both inward and outward currents of amacrine cells in
353 the mouse retina (Horio et al., 2018). The effects of histamine can then be more profound than
354 gain modulation, much as we observed diverse outcomes in RGCs and LGN when different
355 pharmacological and chemogenetic perturbation tools were employed (see also Warwick et
356 al., 2024). Furthermore, in awake conditions, the histaminergic system acts in concert with
357 other neuromodulatory systems (McCormick et al., 2020). For example, serotonergic neurons
358 in the dorsal raphe nucleus have been suggested to project to the retina (Schütte, 1995;
359 Repérant et al., 2000; Gastinger et al., 2006). As the brain state is dynamically controlled by
360 multiple neuromodulators, it will be critical to further characterize neuromodulation of the retina
361 and downstream visual areas in various behavioral contexts.

362 What is the biological relevance of histaminergic modulation of the early visual system,
363 starting at the retina? Growing evidence supports significant correlations between awake
364 retinal responses and various behavioral measures, such as pupil dynamics and locomotion
365 (Schröder et al., 2020; Liang et al., 2020; Boissonnet et al., 2023). We, however, show that
366 resulting changes in pupil size and locomotion behavior by manipulating the histaminergic
367 system were not always consistent with the effects on LGN or RGC visual responses (Figure
368 3). Therefore, the observed changes in their visual responses were unlikely to be associated
369 with behavioral modulation by histamine. This in turn suggests that histamine may not fully
370 explain the fast modulation of RGCs by arousal or locomotion. Additional mechanisms of
371 retinal modulation should then exist, such as the centrifugal serotonergic system (Schütte,
372 1995; Repérant et al., 2000; Gastinger et al., 2006). Further studies on the function of the
373 retina as an integrated part of the whole organism, but not as an isolated tissue, will be critical
374 to better understand sensory information processing in awake animals under natural
375 conditions.

Materials and Methods

No statistical method was used to predetermine the sample size. The significance level was 0.05 (with multiple comparison correction where appropriate) in all analyses unless noted otherwise. All experiments were performed under the license 233/2017-PR and 220/2024-PR from the Italian Ministry of Health, following protocols approved by the Institutional Animal Care and Use Committee at European Molecular Biology Laboratory. The data analyses were done in Python and Matlab.

Animals

Animals were housed on a 12h light-dark cycle, with ad libitum access to water and food. All experiments were performed on female mice. A total of 20 wild-type (C57BL6/J; RRID:IMSR_JAX:000664) and 10 hemizygous HDC-cre (Hdctm1.1(icre)Wwis/J; RRID:IMSR_JAX:021198) mice were used for pharmacological and chemogenetic manipulations, respectively.

Surgical procedures

All surgical procedures were performed in animals from 4 to 19 weeks old (9.2 weeks median age). Before the surgery, animals were injected with Caprofen (5 mg/Kg) and then anaesthetized with isoflurane (4% for induction, 1% for maintenance in O_2). Throughout the surgery, the temperature of the animals was kept stable at 37°C using a heating pad (Supertech Physiological). Ointment (VitA-Pos, Ursapharm) was applied on both eyes to prevent them from drying during the surgery, and the animals were placed in a stereotaxic frame (Stoelting 51625). A portion of the scalp was removed to expose the skull and the periosteum was scraped away with a round scalpel to increase adherence of the dental cement. For those mice belonging to the chemogenetic manipulation group, the skull was aligned in order to level bregma and lambda on the same horizontal plane, and a 100 µm craniotomy was performed using a motorized drill attached to the stereotaxic arm. Viral

401 solution (250 nL; AAV9::FLEX-PSAM Y115F,L141F:5HT3 HC; Vector Biosystems, VB773)
402 was injected with an automatic injector pump at 1nL/sec, at the coordinate of AP: -2.6, ML:
403 ±0.8, DV:-5.3. All animals were then implanted with a custom-made titanium head plate,
404 cemented on the skull using a mixture of cyanoacrylate (Loctite 401, Henkel) and dental
405 cement (Paladur, Kulzer). The head plate featured a hole (8 mm diameter), allowing for clear
406 observation of both bregma and lambda. The skull surface was then glazed with a thick layer
407 of cyanoacrylate in order to support the skull with mechanical, atmospheric and biological
408 protection, while still allowing for visual identification of reference points. After the surgery
409 animals were allowed to recover on a heating pad and then housed in individual cages. During
410 the following seven days, the mice were administered with painkillers (Caprofen) diluted in the
411 drinking water at a concentration of 50 mg/mL.

412 In vivo electrophysiology

413 After recovery from the surgery, animals were habituated to head fixation by placing them in
414 the experimental apparatus over the course of one week, twice a day for up to two hours. On
415 the day of the recording, we first placed the subject animal in the recording set up with its head
416 fixed, and determined the electrode penetration path the target area using the robotic
417 stereotaxic system (StereoDrive, NeuroStar). The animal was then briefly anesthetized (for
418 about 5 minutes) and a hole was drilled around the electrode entry point on the skull. After the
419 removal of the anesthesia, an acute silicone probe (Buzsaki32L, Neuronexus; or P2,
420 Cambridge Neurotech) coated with a fluorescent dye (DiI stain, Invitrogen, D282) was lowered
421 at 5 μm/s using the robotic arm until visual responses were found in the target area.

422 After presenting a battery of visual stimuli, we briefly anesthetized the animal and
423 injected 0.9% saline solution alone or that containing chlorphenamine (H1 antagonist, 5
424 mg/kg), ciproxifan (H3 antagonist, 12 mg/kg), or PSEM (5 mg/kg). About 20 minutes after the
425 injection and removal of the anesthesia, we presented the same battery of visual stimuli to the
426 animal for the second recording session.

427 After all the recording sessions, the electrode position was verified histologically. After
428 retracting the silicon probe, the mice were anesthetized (2.5% Avertin, 16 μL/g, intraperitoneal
429 injection) and perfused with paraformaldehyde (PFA; 4% in phosphate buffer solution). The
430 brain tissue was harvested and post-fixed overnight in 4% PFA at 4°C. Coronal sections of
431 the brain tissue (thickness, 150 μm) were then examined under a fluorescence microscope
432 (Leica, LMD7000 with N2.1 filter cube) to visualize the trace left by the DiI stain on the probe.

433 Visual stimulation

434 Visual stimuli were presented as described before (Boissonnet et al., 2023). Briefly, visual
435 stimuli were projected onto a spherical screen (20cm in radius) painted with ultra-violet (UV)
436 reflective white paint, placed 20 cm from the mouse's left eye. A gamma-corrected digital light
437 processing device (DLP, Texas Instruments, DLPDLCR3010EVM-LC) was used as a light
438 source after the green and the red LEDs were replaced with UV (365nm, LZ1-00UV00, LED
439 Engine) and infrared (IR: 950nm, SFH 4725S, Osram) LEDs respectively. The IR light was
440 used as a synchronization signal and was recorded with a photodiode (PDA100A2, Thorlabs).
441 Stimulation was conducted at 60 frames per second (FPS), and covered 73° in azimuth and
442 44° in altitude from the mouse eye position. The maximum light intensity at the eye position
443 was 31 mW/m^2 (15.4 mW/m^2 for UV LED and 15.9 mW/m^2 for blue LED; measured with S121C
444 sensor, Thorlabs), leading to mesopic to photopic conditions. Using QDSpy software (Franke
445 et al., 2019), we presented the following stimuli: a randomly flickering full-field stimulus (5
446 minutes) consisting of a random sequence of black and white frames at 60 FPS; and a black-
447 and-white binary dense noise stimulus (15 minutes), consisting of a 32-by-18 pixels
448 checkerboard, where each pixel followed an independent random sequence at 60 FPS but the
449 overall luminance of the frame was kept constant at the mean value.

450 Electrophysiology data analysis

451 Raw data from the same animal before and after treatment were concatenated and processed
452 as a single recording. Spike sorting was performed with Kilosort2 for semi-automatic cluster

453 detection and Phy for visualization and data curation. In total, we recorded 311 RGCs from 18
454 animals and 421 cells in LGN from 12 mice.

455 For systematically characterizing the visual response properties, we used stimulus
456 ensemble statistical techniques ("reverse correlation" methods; 500 ms window; Δt = 1/60 s
457 bin size) to calculate the linear filter and static nonlinear gain function of the recorded cells in
458 response to white-noise stimuli as described before (Figure 1A; Boissonnet et al., 2023).
459 Briefly, we first obtained the linear filter of each cell by calculating a spike-triggered average
460 (STA) of the stimulus with ±1 being "white" and "black," respectively. As a quality measure, p-
461 value was computed for each time bin against a null hypothesis that the STA follows a normal
462 distribution with a mean of zero and a variance of 1/C, where C is the total number of spikes.
463 As a measure of the cell's response kinetics, we then estimated the peak latency by fitting a
464 difference-of-Gaussian curve to the linear filter; and the spectral peak frequency by the Fourier
465 analysis on the linear filter. Spatial response properties were examined for STAs from
466 "checkerboard" stimulation. In particular, we fitted a two-dimensional Gaussian envelope to
467 the spatial filter at the peak latency (e.g., Supplementary Figure 3B,H), and the receptive field
468 (RF) size was estimated as twice the mean standard deviation (SD) of the long and short axes.

469 The linear temporal filters from full-field white-noise stimuli were used for broadly
470 classifying the response types of RGCs and LGN cells, respectively (Supplementary Figure
471 1). Specifically, we first used t-Distributed Stochastic Neighbor Embedding (t-SNE) to map the
472 STAs onto two-dimensional space, and then used K-means++ algorithm for heuristically
473 categorizing the responses into the following six types: fast ON, ON, slow ON, fast OFF, OFF,
474 and slow OFF.

475 Static nonlinear gain function of each cell (bin size, 0.1) was computed as: P(response
476 | stimulus) = N(stimulus | response) / N(stimulus) / Δt, where N(stimulus | response) and
477 N(stimulus) are the distributions of spike-triggered stimulus ensembles projected onto the L2-
478 normalized STA and the entire stimulus ensembles, respectively. The ratio of P(response |

479 stimulus) before and after the treatment was used as a measure of response gain modulation
480 for each cell.

481 Behavioral data analysis

482 For all experiments, the mouse's left eye – i.e., the side presented with visual stimuli – was
483 recorded using an IR camera (The Imaging Source, DMK23UV024) to monitor its motion and
484 pupil dynamics at 30-60Hz. Pupil detection was done using a Mask-Region based
485 Convolutional Neural Network (Mask-RCNN), trained as described previously (Boissonnet et
486 al., 2023). Two-dimensional ellipse was fit to the pupil, and the large axis diameter was used
487 as a measure of the pupil size. We then calculated the mean pupil size during the recording
488 sessions, and used the ratio before and after pharmacologic or chemogenetic treatment as a
489 measure of the treatment effects on the pupil dynamics (Figure 3A).

490 We also monitored the running speed of an animal based on the turning speed of the
491 custom-made rotary treadmill throughout the recordings. We set a threshold at 2 cm/s to detect
492 running behavior. The animals, however, did not run frequently on the treadmill (17 ± 25%,
493 mean ± standard deviation; 30 animals). As a measure of the treatment effects, we thus used
494 a) the ratio of the fraction of the "non-running" period (Figure 3B); and b) that of the average
495 running speed during the recording session before and after pharmacological or chemogenetic
496 treatment (Figure 3C).

497 Model analysis

498 To explore how different aspects of neuronal intrinsic properties and output responses are
499 interrelated between each other, we simulated a model neuron's responses to white-noise
500 stimuli using different model parameter values (Figure 4A), and characterized these simulated
501 responses using a linear-nonlinear cascade model as we did for the experimental data.

502 Specifically, we employed an integrate-and-fire neuron model with Poisson spiking and
503 refractoriness. A model neuron's discrete linear filter (of length n_T = 25) was given by a

trigonometric function with logarithmic scale in time: i.e., $L(i) = \sin[2*\pi*((10^{t_i}-1)/(10^{s_t}-1))]$, where $s_t = 1.5$ is a temporal spacing parameter and $t_i = i*s_t/(n_T-1)$ for $i=0,\ldots,n_T-1$. The spike-generating function V(i) was then modelled by first projecting the white-noise Gaussian stimulus S(i) (of length 1,000,000; normalized to have a maximum value of 1) onto L(i), followed by the addition of baseline B and the multiplication by gain G: i.e., $V(i) = G*(\Sigma_j L(j)*S(i-j) + B)$. For each simulation, we chose the value of B from -0.45 to 0.45 in steps of 0.15; and that of G from 1.2^g with g = -3, -2, -1, 0, 1, 2, 3. The spiking response was then generated by thresholding V(i) (at a random threshold for every time point derived from a uniform distribution from 0 to 1) and refractoriness (given by an exponential filter: $-\exp[-i/s_h]$ for i = 0,…,5 with $s_h = 1$). The output spike trains were then subject to the reverse-correlation analysis as described above to characterize the apparent linear filter and static nonlinearity of the model neuron, much as we did for the experimentally recorded RGCs and LGN cells. Specifically, we focused on the peak latency and frequency of the estimated linear filters and the slope of the estimated static nonlinear gain function, and examine how these features depend on the baseline B and the intrinsic gain G of the model neuron (Figure 4B-E).

Acknowledgments

This work was supported by research grants from EMBL (H.A.). The EMBL Advanced Light Microscopy Facility are acknowledged for support in histological image acquisition and analyses, and EMBL IT Support for provision of computer and data storage servers. We thank Dmitry Molotkov, Tom Boissonnet, Vanesa Pelcastre, Sahana Rao, Shabnam Chandel for their help in experiments, and all the Asari lab members for many useful discussions..

References

Bloomfield, S.A., Völgyi, B. (2009). The diverse functional roles and regulation of neuronal gap junctions in the retina. Nat Rev Neurosci. 10(7), 495–506.

Boissonnet, T., Tripodi, M., Asari, H. (2023). Awake responses suggest inefficient dense coding in the mouse retina. Elife. 12, e78005.

Brown, R.E., Sergeeva, O.A., Eriksson, K.S., Haas, H.L. (2002). Convergent Excitation of Dorsal Raphe Serotonin Neurons by Multiple Arousal Systems (Orexin/Hypocretin, Histamine and Noradrenaline). J. Neurosci. 22, 8850–8859.

Chichilnisky, E. J. (2001). A simple white noise analysis of neuronal light responses. Network, 12(2), 199–213.

Durand, S., Iyer, R., Mizuseki, K., de Vries, S., Mihalas, S., Reid, R. C. (2016). A Comparison of Visual Response Properties in the Lateral Geniculate Nucleus and Primary Visual Cortex of Awake and Anesthetized Mice. J Neurosci, 36(48), 12133–12156.

Esposti, F., Johnston, J., Rosa, J. M., Leung, K.-M., Lagnado, L. (2013). Olfactory Stimulation Selectively Modulates the OFF Pathway in the Retina of Zebrafish. Neuron, 79(1), 97-110.

Franke, K., Chagas, A. M., Zhao, Z., Zimmermann, M. J., Bartel, P., Qiu, Y., Szatko, K. P., Baden, T., Euler, T. (2019). An arbitrary-spectrum spatial visual stimulator for vision research. Elife, 8, e48779.

Gastinger, M.J., O'Brien, J.J., Larsen, J.N.B., Marshak, D.W. (1999). Histamine Immunoreactive Axons in the Macaque Retina. Invest. Ophthalmol. Vis. Sci. 40, 487–495.

Greferath, U., Kambourakis, M., Barth, C., Fletcher, E.L., Murphy, M. (2009). Characterization of histamine projections and their potential cellular targets in the mouse retina. Neuroscience 158, 932–944.

Gastinger, M. J., Tian, N., Horvath, T., Marshak, D. W. (2006). Retinopetal axons in mammals: Emphasis on histamine and serotonin. Curr. Eye Res. 31, 655–667.

Haas, H., Panula, P. (2003). The role of histamine and the tuberomamillary nucleus in the nervous system. Nat. Rev. Neurosci. 4, 121–130.

553 Horio, K., Ohkuma, M., Miyachi, E.-I. (2018). The effect of histamine on inward and
554 outward currents in mouse retinal amacrine cells. Cell. Mol. Neurobiol. 38, 757–767.

555 John, J., Wu, M.-F., Boehmer, L.N., Siegel, J.M. (2004). Cataplexy-Active Neurons in the
556 Hypothalamus: Implications for the Role of Histamine in Sleep and Waking Behavior.
557 Neuron 42, 619–634.

558 Kamei, C., Okumura, Y., Tasaka, K. (1993). Influence of histamine depletion on learning
559 and memory recollection in rats. Psychopharmacology (Berl.) 111, 376–382.

560 Khateb, A., Fort, P., Pegna, A., Jones, B.E., Mühlethaler, M. (1995). Cholinergic nucleus
561 basalis neurons are excited by histamine in vitro. Neuroscience 69, 495–506.

562 Khouma, A., Moeini, M.M., Plamondon, J., Richard, D., Caron, A., Michael, N.J. (2023).
563 Histaminergic regulation of food intake. Front. Endocrinol. 14.

564 Klapdor, K., Hasenöhrl, R.U., Huston, J.P. (1994). Facilitation of learning in adult and aged
565 rats following bilateral lesions of the tuberomammillary nucleus region. Behav. Brain Res.
566 61, 113–116.

567 Labandeira-Garcia, J.L., Guerra-Seijas, M.J., Gonzalez, F., Perez, R., Acuña, C., (1990).
568 Location of neurons projecting to the retina in mammals. Neurosci. Res. 8, 291–302.

569 Lee, S.-H., Dan, Y. (2012). Neuromodulation of Brain States. Neuron 76, 209–222.

570 Liang, L., Fratzl, A., Reggiani, J.D.S., El Mansour, O., Chen, C., Andermann, M.L. (2020).
571 Retinal Inputs to the Thalamus Are Selectively Gated by Arousal. Curr. Biol. CB 30, 3923–
572 3934.e9.

573 Lin, W., Xu, L., Zheng, Y., An, S., Zhao, M., Hu, W., Li, M., Dong, H., Li, A., Li, Y., Gong,
574 H., Pan, G., Wang, Y., Luo, Q., Chen, Z. (2023) Whole-brain mapping of histaminergic
575 projections in mouse brain. Proc. Natl. Acad. Sci. U. S. A. 120, e2216231120.

576 Magnus, C.J., Lee, P.H., Bonaventura, J., Zemla, R., Gomez, J.L., Ramirez, M.H., Hu, X.,
577 Galvan, A., Basu, J., Michaelides, M., Sternson, S.M. (2019). Ultrapotent chemogenetics
578 for research and potential clinical applications. Science. 364(6436), eaav5282

579 McCormick, D.A., Nestvogel, D.B., He, B.J., (2020). Neuromodulation of brain state and
580 behaviour. Ann. Rev. Neurosci. 43(1), 391–415.

581 McCormick, D.A., Williamson, A. (1991). Modulation of neuronal firing mode in cat and
582 guinea pig LGNd by histamine: possible cellular mechanisms of histaminergic control of
583 arousal. J. Neurosci. 11 (10), 3188–3199.

584 Mochizuki, T., Yamatodani, A., Okakura, K., Horii, A., Inagaki, N., Wada, H. (1992).
585 Circadian rhythm of histamine release from the hypothalamus of freely moving rats.
586 Physiol. Behav. 51, 391–394.

587 Orsetti, M., Ghi, P., Carlo, G.D. (2001). Histamine H3-receptor antagonism improves
588 memory retention and reverses the cognitive deficit induced by scopolamine in a two-trial
589 place recognition task. Behav. Brain Res. 124, 235–242.

590 Parmentier, R., Ohtsu, H., Djebbara-Hannas, Z., Valatx, J.-L., Watanabe, T., Lin, J.-S.
591 (2002). Anatomical, Physiological, and Pharmacological Characteristics of Histidine
592 Decarboxylase Knock-Out Mice: Evidence for the Role of Brain Histamine in Behavioral
593 and Sleep–Wake Control. J. Neurosci. 22, 7695–7711.

594 Pierce, M.E., Sheshberadaran, H., Zhang, Z., Fox, L.E., Applebury, M.L., Takahashi, J.S.
595 (1993). Circadian regulation of iodopsin gene expression in embryonic photoreceptors in
596 retinal cell culture. Neuron 10, 579–584.

597 Reggiani, J.D.S., Jiang, Q., Barbini, M., Lutas, A., Liang, L., Fernando, J., Deng, F., Wan,
598 J., Li, Y., Chen, C., Andermann, M.L. (2023). Brainstem serotonin neurons selectively gate
599 retinal information flow to thalamus. Neuron 111, 711–726.e11.

600 Repérant, J., Médina, M., Ward, R., Miceli, D., Kenigfest, N.B., Rio, J.P., Vesselkin, N.P.
601 (2007). The evolution of the centrifugal visual system of vertebrates. A cladistic analysis
602 and new hypotheses. Brain Res. Rev. 53, 161–197.

603 Repérant, J., Araneda, S., Miceli, D., Medina, M., Rio, J. P. (2000). Serotonergic
604 retinopetal projections from the dorsal raphe nucleus in the mouse demonstrated by
605 combined [3H] 5-HT retrograde tracing and immunolabeling of endogenous 5-HT. Brain
606 Res. 878, 213–217.

607 Rubio, S., Begega, A., Santin, L.J., Arias, J.L. (2002). Improvement of spatial memory by
608 (R)-α-methylhistamine, a histamine H3-receptor agonist, on the Morris water-maze in rat.
609 Behav. Brain Res. 129, 77–82.

610 Scammell, T.E., Jackson, A.C., Franks, N.P., Wisden, W., Dauvilliers, Y. (2018).
611 Histamine: neural circuits and new medications. Sleep 42, zsy183.

612 Schröder, S., Steinmetz, N.A., Krumin, M., Pachitariu, M., Rizzi, M., Lagnado, L., Harris,
613 K.D., Carandini, M. (2020). Arousal Modulates Retinal Output. Neuron 107, 487–495.e9.

614 Schütte, M. (1995). Centrifugal innervation of the rat retina. Vis. Neurosci. 12, 1083–1092.

615 Takahashi, K., Lin, J.-S., Sakai, K. (2006). Neuronal activity of histaminergic
616 tuberomammillary neurons during wake-sleep states in the mouse. J. Neurosci. Off. J. Soc.
617 Neurosci. 26, 10292–10298.

618 Thakkar, M.M. (2011). Histamine in the regulation of wakefulness. Sleep Med Rev. 15(1),
619 65-74.

620 Uhlrich, D. J., Manning, K. A., Xue, J.-T.. (2002). Effects of activation of the histaminergic
621 tuberomammillary nucleus on visual responses of neurons in the dorsal lateral geniculate
622 nucleus. J. Neurosci. 22, 1098–1107.

Valdés, J.L., Sánchez, C., Riveros, M.E., Blandina, P., Contreras, M., Farías, P., Torrealba, F. (2010). The histaminergic tuberomammillary nucleus is critical for motivated arousal. Eur. J. Neurosci. 31, 2073–2085.

van Ruitenbeek, P., Vermeeren, A., Smulders, F.T.Y., Sambeth, A., Riedel, W.J. (2009). Histamine H1 receptor blockade predominantly impairs sensory processes in human sensorimotor performance. Br. J. Pharmacol. 157, 76–85.

Wang, Y.-Q., Li, R., Wu, X., Zhu, F., Takata, Y., Zhang, Z., Zhang, M.-Q., Li, S.-Q., Qu, W.-M. (2015). Fasting activated histaminergic neurons and enhanced arousal effect of caffeine in mice. Pharmacol. Biochem. Behav. 133, 164–173.

Warwick, R.A., Riccitelli, S., Heukamp, A.S., Yaakov, H., Swain, B.P., Ankri, L., Mayzel, J., Gilead, N., Parness-Yossifon, R., Di Marco, S., Rivlin-Etzion, M. (2024). Top-down modulation of the retinal code via histaminergic neurons of the hypothalamus. Sci Adv. 10(35):eadk4062.

Wilson, M., Lindstrom, S.H. (2011). What the bird's brain tells the bird's eye: the function of descending input to the avian retina. Vis Neurosci, 28(4), 337–350.